Thermodynamic optimization of Organic Rankine Cycle architectures for waste heat recovery

Steven Lecompte[a], Henk Huisseune[a], Martijn van den Broek[a], Michel De Paepe[a]

[a]Department of Flow, Heat and Combustion Mechanics, Ghent University, Sint-Pietersnieuwstraat 41, 9000 Gent ,Belgium, steven.lecompte@ugent.be, CA, henk.huisseune@ugent.be, martijn.vandenbroek@ugent.be ,michel.depaepe@ugent.be

Abstract:

Organic Rankine cycles (ORC) are a well proven technology in the waste heat recovery market. The conventional ORC typically operates in subcritical conditions and optionally includes a recuperator. Yet, performance gains to the basic configuration are attainable by introducing cycle modifications. Alternative cycles, which maintain the same component arrangement as the subcritical ORC, are the transcritical and the partial evaporation cycle. These three cycle configurations are systematically analysed in this work. The partial evaporation cycle is a generalization of the triangular cycle. An exergy analysis highlights the potential of each of the alternative cycle architectures. A robust optimization scheme is set up by introducing dimensionless parameters. The heat carrier temperature varies between 100 °C and 350 °C. The condenser cooling water inlet temperature ranges between 15 °C and 30 °C. In total 67 working fluids are considered. Special care was taken to assess the implication of various design constraints. For low heat carrier inlet temperatures (140 °C), the alternative cycles have relative increased exergy efficiencies by up to 18,5% compared to the basic optimized subcritical ORC. However, for high heat carrier temperatures the performance gain becomes small. In a second step the effect of expander design constraints are analysed. The reported results are helpful as guidelines in ORC system development.

Keywords:

ORC, cycle architectures, optimization, transcritical, triangular, subcritical, working fluids

1. Introduction

The ORC is a well proven technology for converting low temperature/low capacity heat to electricity. Cost-effective solutions have been demonstrated for waste heat recovery, geothermal, solar and biomass applications. The current state-of-the-art technology typically consists of a subcritical ORC, sometimes complemented with a recuperator. For a list of commercially available systems we refer to the work of Tchanche et al. [1].

However, alternative cycle architectures have the potential to improve the thermodynamic performance. Performance gains can amongst others be found for multi-pressure cycles (MPORC) [2-4], triangular (TLC) [5-9] and transcritical cycles (TCORC) [5, 10-13]. The last two cycles architectures will be further investigated as these have a basic component layout identical to the subcritical ORC (SCORC), only the operational regime is different. In this work also the partial evaporation cycle (PEORC) [14] is investigated. This cycle is a hybrid between the TLC and subcritical cycle. The working fluid in the PEORC enters the turbine in a state between saturated liquid and saturated vapour.

In the scientific literature there is no consensus on the best performing cycle architecture. This is due to two main reasons. First, throughout the various papers published, different assumptions and boundary conditions are used. This makes a direct comparison impossible. Secondly, several works introduce a preselection of the working fluids. This preselection can be based on environmental, technical or safety constraints. High performing cycles can have been excluded due to missing adequate working fluids. By doing the screening in a post-processing step, recommendations for

new fluids can be made. These new fluids should then additionally comply with added e.g. environmental, safety and technical constraints.

A subsequent challenge is to identify the financial feasibility. This however does not fall within the scope of the current paper. The goal of this work is to set a baseline for possible thermodynamic improvement by using modified cycle architectures. With this knowledge a first assessment can already be made whether alternative architectures can result in improved ORC systems.

2. Methodology

The focus of the presented analysis is on waste heat recovery applications. The heat after the ORC is not used for heating purposes. Furthermore, there is no limit on the exit temperature of the heat carrier after the evaporator. Therefore the main objective is to maximize the net electrical power output of the ORC from a given waste heat stream.

2.1. Cycle architectures under investigation

Three cycle architectures are investigated in this work: the subcritical ORC (SCORC), the transcritical ORC (TCORC), and the partial evaporation ORC (PEORC). The TLC is considered a subset of the PEORC. The component layout for the three cycles is identical and given in Fig. 1. The T-s diagram for the three cycles is presented in Fig. 2. These two figures also introduce the nomenclature used. The main components are the evaporator, expander, condenser and pump, completed by the working fluid.

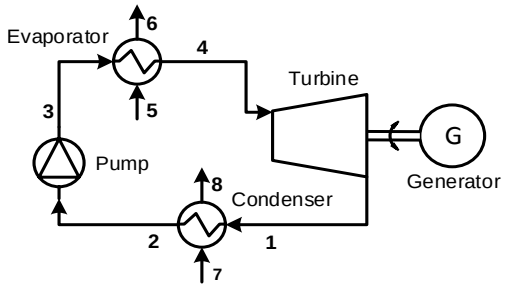

Fig. 1. Component layout of the ORC architectures under consideration.

The basic SCORC is explained with the help of Fig. 1. First, the hot working fluid leaving the turbine (1) is condensed in the condenser. The heat from the condensation process is transferred to a cooling loop (7-8) which typically consists of water or air. Subsequently, the condensed working fluid enters (2) the pump and is pressurized (3). Then, the working fluid enters the evaporator and is heated to a superheated state (4). The temperature of the heat carrier (5-6) is gradually reduced in this process. The superheated vapour (4) enters the turbine producing work. This cycle is again repeated starting from (1).

For a transcritical cycle the evaporator is typically called the vapour generator as the two-phase state is omitted. For the TLC only the pre-heating section remains while for a PEORC the working fluid evaporates to a state between saturated liquid and saturated vapour.

2.2. Model and cycle assumptions

The cycle parameters used for characterizing the cycle are shown in Table 1. The cycles are modelled under the assumption of steady state operation. Furthermore, heat losses to the environment and pressure drops in the heat exchangers are considered negligible. Details about the modelling approach are elaborated in a previous work [15]. A discretization approach is implemented for modelling the heat exchangers. The evaporators are segmented into N parts. As such, changing fluid properties are taken into account. This is particularly essential for the TCORC vapour generator. When changing N=20 to N=100 the calculated net power output of the TCORC changes less than 0.1 % and this for all cases under consideration. Thus, to keep the calculation time

acceptable N=20 segments is chosen. For the condenser, the discretization only consists of three zones: superheated, condensing and subcooled zone.

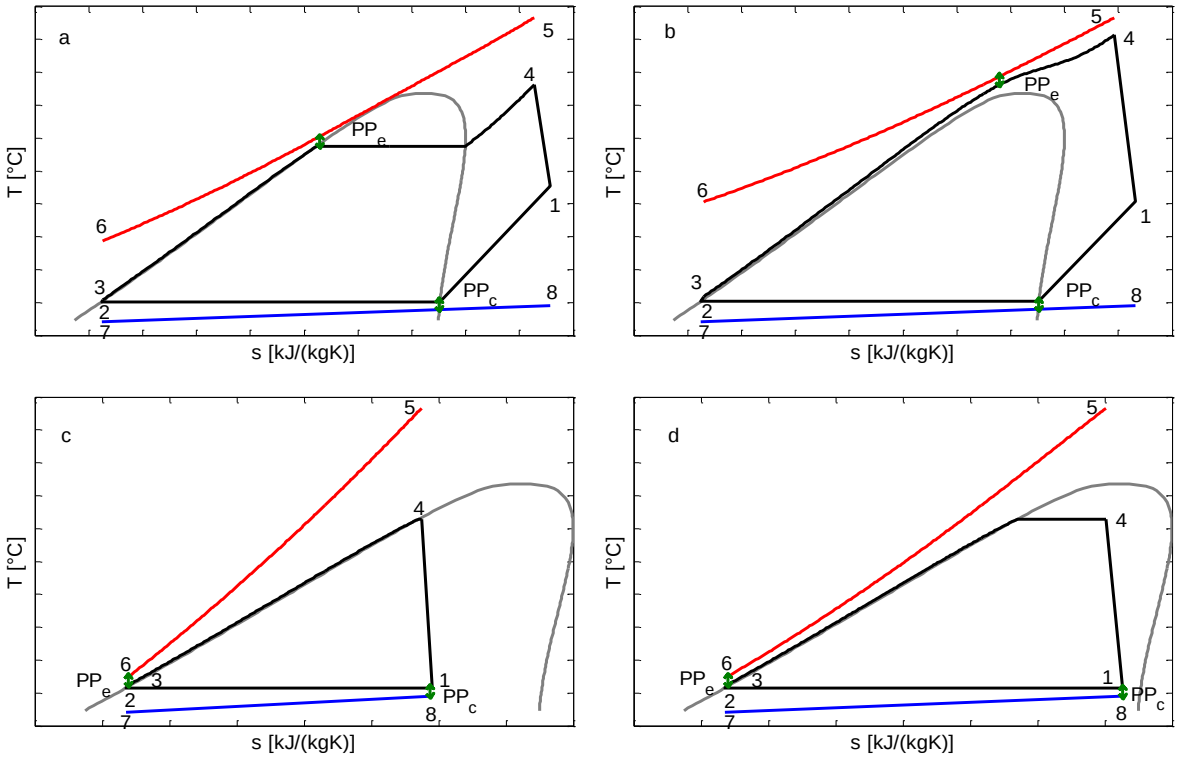

Fig. 2. Ts diagrams of (a) SCORC, (b) TCORC, (c) TLC, (d) PEORC.

The thermophysical data is obtained from CoolProp 4.2.3 [16]. Only pure working fluids are considered, working fluid mixtures are out of scope. The working fluids under consideration all have a critical temperature above 60 °C to make sure two-phase condensation occurs. As such 67 working fluids remain. Furthermore, for the SCORC the maximum pressure is 0.9 times the critical pressure [15, 17]. This to avoid unstable operation in near critical conditions. For the SCORC and TCORC the expansion process should end at a superheated state.

The total heat input to the cycle is given by:

$$\dot{Q}_{evap} = \sum_{i=1}^{N} (h_{wf,e,(x+1)} - h_{wf,e,x}) \dot{m}_{wf} \tag{1}$$

The turbine and pump are modelled by their isentropic efficiency:

$$\dot{W}_{turbine} = (h_{turbine,in} - h^{isentropic}_{turbine,out}) \eta_{turbine} \dot{m}_{wf} \tag{2}$$

$$\dot{W}_{pump} = \frac{h^{isen}_{pump,out} - h_{pump,in}}{\eta_{pump}} \dot{m}_{wf} \tag{3}$$

The net power output is given as:

$$\dot{W}_{net} = \dot{W}_{turbine} - \dot{W}_{pump} \tag{4}$$

And the thermal efficiency as:

$$\eta_I = \frac{\dot{W}_{net}}{\dot{Q}_{in}} \tag{5}$$

Table 1. Thermodynamic cycle parameters.

Parameter	Description	Value
η_{pump}	Isentropic efficiency pump [%]	70
$\eta_{turbine}$	Isentropic efficiency turbine [%]	80
PP_e	Pinch point temperature difference in evaporator [°C]	5
PP_c	Pinch point temperature difference in condenser [°C]	5
T_5	Heat carrier inlet temperature [°C]	100-350
T_2	Cooling loop inlet temperature [°C]	15-30
ΔT_{cf}	Cooling loop temperature rise [°C]	10
$\dot{m}_{hf}$	Mass flow rate heat carrier [kg/s]	1

2.3. Assessment criteria

The assessment of the cycles is based on an exergy analysis. The dead state (p_0, T_0) is in this work defined as the inlet temperature of the condenser cooling loop. When the system reaches thermal, chemical and mechanical equilibrium with the dead state the work potential is zero. The specific exergy *e* for a steady state stream, assuming potential and kinetic contributions are negligible, is defined as:

$$e = h - h_o - T_0(s - s_0) \tag{6}$$

By multiplying the specific exergy with the mass flow rate, the exergy flow $\dot{E}$ is obtained:

$$\dot{E} = \dot{m}e \tag{7}$$

The control volume exergy rate balance for a steady state system is given as:

$$0 = \frac{dE}{dt} = \sum_j (1 - \frac{T_0}{T_j})\dot{Q}_j + \sum_{in} \dot{m}_{in} e_{in} - \sum_{out} \dot{m}_{out} e_{out} - \dot{E}_w - \dot{I}_{component}\,, \tag{8}$$

with $\dot{E}_w = (\dot{W} - p_0 \frac{dV}{dt})$ the exergy transfer rate associated with the transfer of energy by work (except flow work). The exergy destruction is indicted by $\dot{I}_{component}$. The index j refers to an equal temperature section on the boundary of the control volume and $\dot{Q}_j$ is the heat flow rate over the control volume associated to this section.

The second law efficiency is defined as:

$$\eta_{II} = \frac{\dot{W}_{net}}{\dot{E}_{hf,in}} \tag{9}$$

The exergy content of the system can also be written as:

$$1 = \eta_{II} + y_{L,hf,out} + y_{L,cf,out} + y_{D,pump} + y_{D,turbine} + y_{D,condensor} + y_{D,evaporator} \tag{10}$$

With y_L and y_D respectively the exergy loss and destruction ratio:

$$y_L = \frac{\dot{E}_{stream}}{\dot{E}_{hf,in}} \tag{11}$$

$$y_D = \frac{\dot{I}_{component}}{\dot{E}_{hf,in}} \tag{12}$$

Exergy loss, subscript L, is identified as exergy which is unused and discarded into the atmosphere. In this work the two main sources of exergy loss are the exergy at the hot stream outlet of the evaporator, $\dot{E}_{hf,out}$, and at the cooling fluid outlet of the condenser, $\dot{E}_{cf,out}$. Exergy destruction, subscript D, is specified as exergy which is unavoidably lost in the cycle during the conversion from heat to electricity. These are the irreversibilities during finite temperature heat transfer and irreversibilities associated to conversion of mechanical work (pump and expander).
Besides the thermodynamic criteria, technical criteria concerning the expander are formulated. These are the turbine size factor SF (eq. 13), for turbines and the volume coefficient VC (eq. 14), for volumetric expanders.

$$SF = \frac{\dot{V}^{0.5}}{\Delta H_{isen}^{0.25}} \tag{13}$$

$$VC = \frac{v_{\exp,out}}{h_{in,\exp} - h_{out,\exp}} \tag{14}$$

General design ranges can be associated to both parameters, providing a rough means for discarding alternative cycle architectures and working fluids. In refrigeration and heat pump applications the VC ratio is typically between 0.25 and 0.6 m³/MJ, while the SP ratio is typically between 0.02 and 1 m for both subcritical and transcritical cycles [18].

2.4. Optimization strategy

Two degrees of freedom are left for the thermodynamic optimization of the cycle. Depending on the cycle architecture these are:

- The superheating and evaporation pressure (SCORC).
- The vapour quality and evaporation pressure (PEORC).
- The turbine inlet temperature and supercritical pressure (TCORC).

However, in order to support a continuous transition from one cycle architecture to the other, two dimensionless parameters F_p and F_s are introduced. The benefit of using these parameters is that the whole search space can be defined by only two unique parameters. Both have a range [0,1], their definition is given below:

$$F_p = \frac{p_{wf,e} - p_{\min}}{p_{\max} - p_{\min}}, \tag{15}$$

$$p_{\max} = 1.3 p_{wf,crit} \qquad T_5 - PP_e > T_{wf,crit} \tag{16}$$

$$p_{wf,sat}(T = T_5 - PP_e) \qquad T_5 - PP_e < T_{wf,crit} \tag{17}$$

$$p_{\min} = p_{wf,sat}(T = T_8 + PP_c) \tag{18}$$

and

$$F_s = \frac{s_4 - s_{\min}}{s_{\max} - s_{\min}}, \tag{19}$$

$$s_{\min} = s_{wf,sat,liq}(p = p_{wf,e}) \qquad p_{wf,e} < p_{wf,crit} \tag{20}$$

$$s_{\min} = s_{wf,crit} \qquad p_{wf,e} > p_{wf,crit} \tag{21}$$

$$s_{\max} = s_{wf}(p = p_{wf,e}, T = T_5 - PP_e) \tag{22}$$

F_s and F_p encompasses the envelope in which an ORC can be designed. The F_p parameter directly fixes the evaporation pressure. A value of zero corresponds to the condensation temperature corrected with the pinch point temperature difference. The maximum of one corresponds to a heat carrier input temperature corrected with the pinch point temperature difference or $1.3P_{crit}$ for a TCORC. The parameter F_s determines the amount of superheating (SCORC), the vapour quality (TLC) or the turbine inlet temperature (TCORC). A value of zero corresponds to a saturated liquid state or the critical point for a TCORC. The maximum of one, gives a pinch point located at the heat carrier inlet.

An example of the resulting second law efficiency η_{II} in function of F_p and F_s is given in Fig. 3. The working fluid used is R245fa with a waste heat inlet temperature $T_5 = 200$ °C and a cooling loop inlet temperature $T_7 = 20$ °C. The three regions bordered by a black line correspond with the PEORC, SCORC and TCORC. For his case it is clear that a minimum superheating for a SCORC results in the highest second law efficiency. The TCORC attains the highest η_{II} of 0.57.

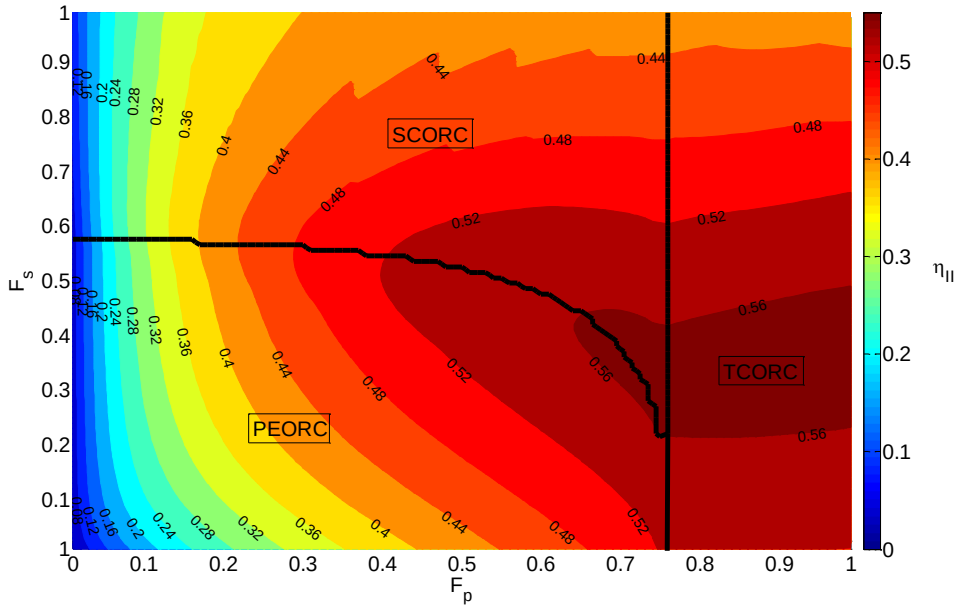

Fig. 3. Second law efficiency η_{II} in function of F_p and F_s for $T_5 = 200$ °C and $T_7 = 20$ °C.

A multistart algorithm [19] searches the global maximum of the second law efficiency ($\eta_{II,\max}$) for a group T_5 = [100, 120, 140, 160, 180, 200, 225, 250, 275, 300, 325, 350] °C, T_7 = [15, 20, 25, 30] °C by optimizing both parameters F_p and F_s. First, a set of 40 randomly distributed start points are generated. Subsequently, a local solver based on a trust-region algorithm [20] starts at these trail points and the best solution is retained.

3. Results and discussion

3.1. Optimal set of working fluids

In Fig. 4 the results of the optimization strategy are plotted. Besides the calculated points (a total of 48), surface fits generated from the data are shown. These surface fits take the form:

$$\eta_{II,\max} = a + \frac{b(cT_2 + 1)}{(dT_5 + 1)} \tag{7}$$

The used regression model captures the trends of the data well with R^2 values of respectively 0.990, 0.988 and 0.998 for the SCORC, TCORC and PEORC. These simple regression models could be used to quickly asses the benefits of alternative cycle architectures. The corresponding working fluids are listed in Appendix A.

The PEORC clearly shows the highest second law efficiency followed by the TCORC and SCORC. At (T_5=140 °C, T_7=15 °C) the maximum second law efficiency $\eta_{II,\max}$ is 0.469, 0.504 and 0.557 for respectively the SCORC, TCORC and PEORC.

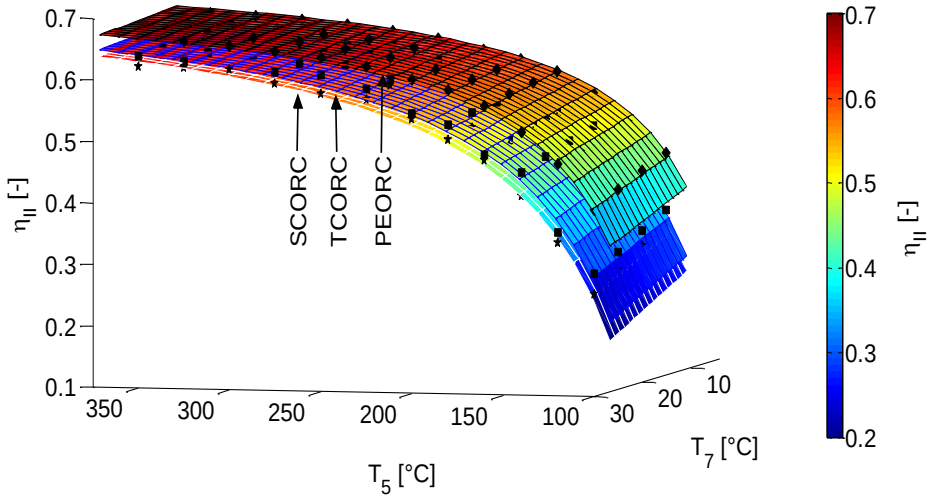

Fig.4. Maximum second law efficiency η_{II} for SCORC, TCORC and PEORC.

Furthermore, two principal remarks can be made. First, the relative difference in $\eta_{II,\max}$ between a TCORC and SCORC is much smaller than between the PEORC and SCORC. At (T_5 =140 °C, T_7 = 15 °C) the PEORC outperforms the SCORC by 18.76 % while for these conditions the TCORC only shows an increased second law efficiency of 7.46 %. Second, for increasing heat carrier inlet temperature T_5 the benefits of going to a TCORC or PEORC decrease. For example, at (T_5=300°C, T_7 = 15 °C) the TCORC and PEORC respectively show only an increased second law efficiency of 1.12 % and 5.1 %. The reported values are valuable to define an upper region in which a feasible ORC design can be found. In section 3.3, the effects of additional constraints related to the expander technology are investigated.

3.2. Exergy content

The exergy content in the cycle is depicted in Fig. 5. For the SCORC at temperatures $T_5 > 180$ °C, the turbine exergy destruction accounts for the largest exergy share. For low temperatures T_5, the sum of both the evaporator exergy destruction and losses are dominant. Thus, for high heat carrier temperatures this justifies the focus on development of high performant expander technology. While for low temperatures novel ways of efficiently capturing the available exergy is key. The higher second law efficiency $\eta_{II,\max}$ of the TCORC and PEORC follows from the lower evaporator exergy destruction $Y_{D,evaporator}$ and losses $Y_{L,evaporator}$. Yet, for low heat carrier inlet temperatures T_5 there is no good supercritical working fluid which significantly reduces $Y_{L,evaporator}$. The PEORC on the other hand clearly shows lower $Y_{L,evaporator}$. If there is a lower cooling limit on the heat carrier, the benefit of the PEORC is evidently offset.

Furthermore, as expected, the exergy destruction by the pump is consistently larger for the TCORC compared to the SCORC and PEORC.

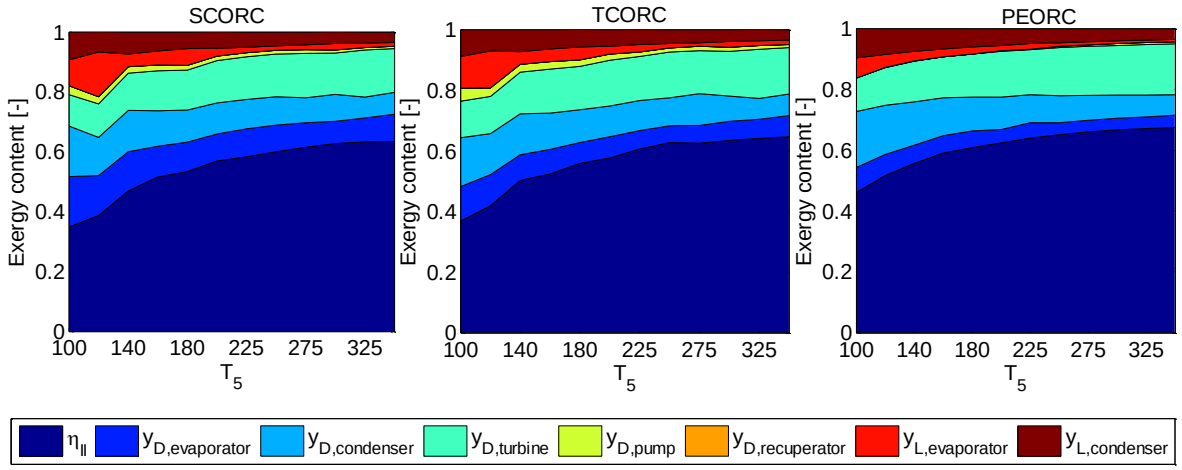

Fig.5. Maximum second law efficiency $\eta_{II,\max}$ *for SCORC, TCORC and PEORC at* $T_7 = 15\,°C$.

3.3. Thermodynamic expander criteria

In this section, the volume coefficient (VC) and size factor (SF) resulting from the optimization are examined.

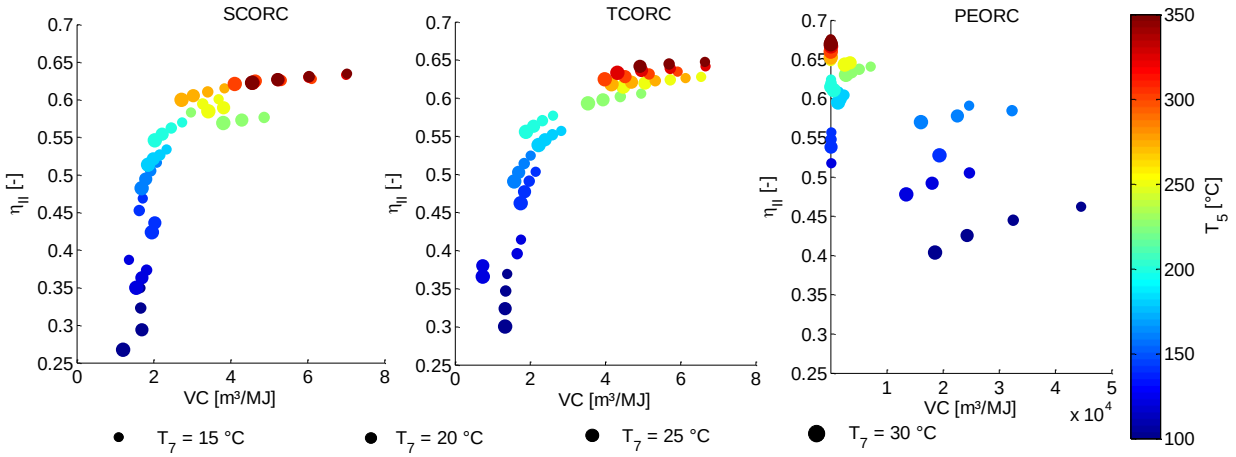

Fig.6. Volume coefficient (VC) at $\eta_{II,\max}$ *for SCORC, TCORC and PEORC.*

The VC for the three architectures under consideration are plotted in Fig. 6. Both the SCORC and TCORC exhibit a similar trend. A decrease in T_5 and increase in T_7 result in a reduction of VC. Starting around T_5 = 200 °C the VC increases sharply. Therefore, implementing high efficiency single stage volumetric expanders becomes technically difficult for high temperature heat carriers. The PEORC shows very large volume coefficients of up to 44580 m³/MJ for low T_5. Increasing T_5 to 250 °C decreases the VC to values of 50 m³/MJ. Yet, the values reported for the PEORC are at least 5 times larger than for the SCORC and TCORC.

The size factor is plotted in Fig 7. For the SCORC the values of SF lie between 0.014 and 0.029 m. For the TCORC the trend is similar, but the SF is slightly lower with values between 0.0140 and 0.022 m. For the PEORC the SF lies between 0.006 and 0.16m. However, all of the PEORC cycles end or go through the two phase region. Thus the risk of turbine blade erosion is considerable.

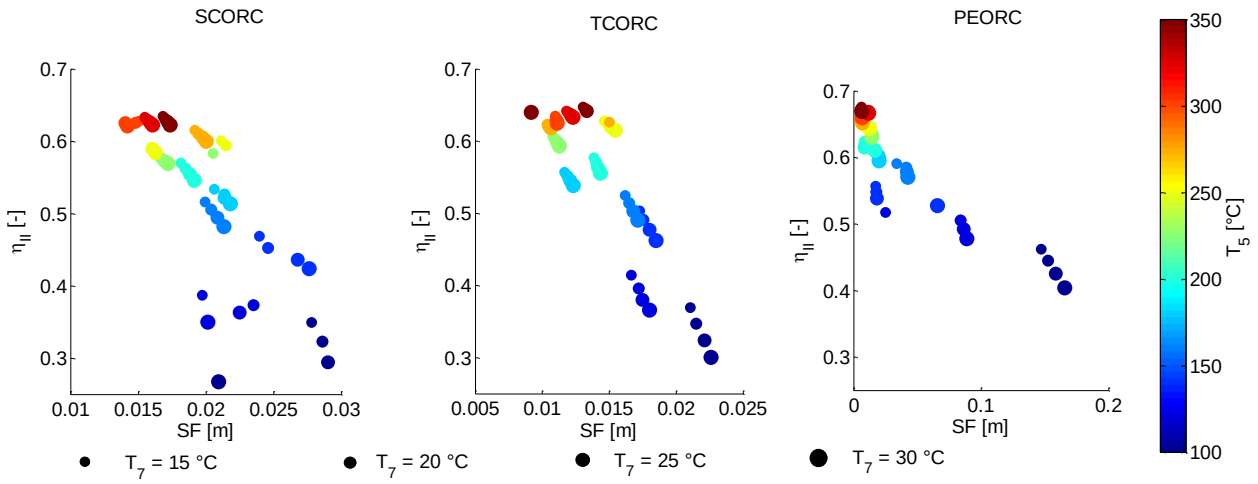

Fig.7. Size factor (SF) at $\eta_{II,\max}$ for SCORC, TCORC and PEORC.

Only the small subset consisting of $\eta_{II,\max}$ was discussed above. However, all 67 working fluids in combination with each of the three cycle architectures were optimized. These calculations provide a complete map for selecting working fluid and cycle architectures taking expander constraints into account. For each T_5 and T_7 there are working fluids which satisfy custom expander constraints but at the cost of a decreased η_{II}. For example, the PEORC at $\eta_{II,\max}$ and T_5 = 250 °C had a VC around 50 m³/MJ, however the VC can be significantly reduced in detriment of decreased η_{II} as shown in Fig. 8. The generated dataset can thus be used to make a pre-selection of working fluids and corresponding cycle architectures for specific case studies. The final optimal sizing subsequently follows from thermo-economic considerations.

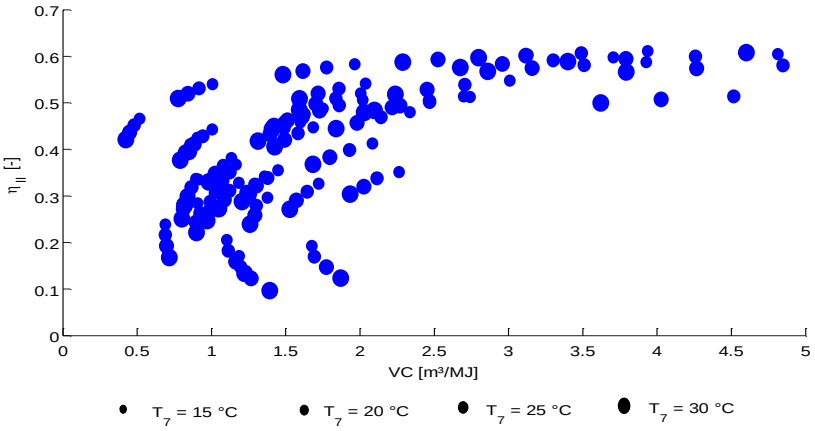

Fig.8. Volume coefficient (VC) in function of η_{II} for the PEORC at T_5 = 250 °C considering all 67 working fluids.

4. Conclusion

In the presented work, a general thermodynamic optimization framework for ORCs is proposed. First, the potential thermodynamic improvement by using modified ORC architectures is investigated. The subcritical, partial evaporation and transcritical cycle were investigated. Under the condition of maximum second law efficiency simple regression models with a good fit are formulated. These simple regression models can be used to quickly compare cycle architectures. Furthermore, under all simulated heat carrier and cooling loop temperatures the TCORC and PEORC show increased second law efficiency compared to the SCORC. However, for increasing heat carrier inlet temperature the difference between the SCORC and the alternative cycles

diminishes. For example, at a heat carrier inlet temperature of 140 °C, the relative increase in second law efficiency over a subcritical cycle is 7.46% and 18.76% for respectively the TCORC and PEORC. For a heat carrier inlet temperature of 300 °C this reduces to 1.12% and 5.1% for respectively the TCORC and PEORC.

Additionally, feasible cycle designs should adhere to limitations considering the expander design. Especially for the PEORC the design of a volumetric machine is challenging due to the high volumetric coefficient under maximisation of the second law efficiency. Therefore the expander evaluation criteria in function of the second law efficiency for each of the cycle architectures and working fluids under consideration were calculated. From this, it is clear that technical expander design constraints can be satisfied in detriment of decreased second law efficiency. The optimization framework can thus be used to make a pre-selection of cycle architectures and corresponding working fluids for specific ORC applications. The final optimal sizing subsequently follows from thermo-economic considerations.

Acknowledgments

The results presented in this paper have been obtained within the frame of the IWT SBO-110006 project The Next Generation Organic Rankine Cycles (www.orcnext.be), funded by the Institute for the Promotion and Innovation by Science and Technology in Flanders. This financial support is gratefully acknowledged.

Nomenclature

$\dot{E}$	flow exergy, W
e	specific exergy, J/kg
h	specific enthalpy, J/kg
$\dot{m}$	mass flow rate, kg/s
p	pressure, Pa
PP	pinch point temperature difference, °C
$\dot{Q}$	rate of heat flow, W
s	entropy, J/kg K
SF	size factor, m
T	temperature, °C
v	specific volume, m³/kg
VC	volume coefficient, m³/MJ
y_L	exergy loss ratio, -
y_D	exergy destruction ratio, -

Greek symbols

η	efficiency

Subscripts and superscripts

I	first law
II	second law
c	condenser
e	evaporator
cf	cold fluid
crit	critical

hf	heat carrier fluid
liq	liquid
sat	saturated
wf	working fluid

Abbreviations

SCORC	subcritical ORC
TCORC	transcritical ORC
PEORC	partial evaporation ORC
TLC	triangular cycle

Appendix A

Table A1. Optimal set of working fluids for SCORC

T_5|T_7 °C	15	20	25	30
100	R218	R218	R218	R143a
120	R1234yf	R227ea	R227ea	R227ea
140	R227ea	R227ea	RC318	RC318
160	R236fa	R236fa	R236fa	R236fa
180	R114	R114	R114	R114
200	R245fa	R245fa	R245fa	R245fa
225	R1233zde	R365mfc	R365mfc	R365mfc
250	R123	R123	n-pentane	n-pentane
275	R141b	R141b	R141b	R141b
300	Cyclopentane	Cyclopentane	Cyclopentane	Cyclopentane
325	Acetone	Acetone	Acetone	Acetone
350	Acetone	Acetone	Acetone	Acetone

Table A2. Optimal set of working fluids for TCORC

T_5|T_7 °C	15	20	25	30
100	R218	R218	R218	R218
120	R227ea	R227ea	R143a	R143a
140	RC318	RC318	RC318	RC318
160	R236fa	R236fa	R236fa	R236fa
180	Neopentane	Neopentane	Neopentane	Neopentane
200	R245fa	R245fa	R245fa	R245fa
225	n-pentane	n-pentane	n-pentane	n-pentane
250	R113	R113	R113	R113
275	R113	Cyclopentane	Cyclopentane	Cyclopentane
300	Cyclopentane	Cyclopentane	Cyclopentane	Cyclopentane
325	Acetone	Acetone	Acetone	Acetone
350	Acetone	Acetone	Acetone	Acetone

Table A3. Optimal set of working fluids for PEORC

T_5|T_7 °C	15	20	25	30
100	MD3M	MD3M	MD3M	MD3M
120	Water	MD3M	MD3M	MD3M
140	Water	Water	Water	D6
160	MD3M	D6	D6	D6
180	D4	MD2M	MD2M	MD2M
200	Water	Water	Water	D4
225	n-Dodecane	n-Dodecane	n-Dodecane	n-Dodecane
250	Water	Water	n-Dodecane	n-Dodecane
275	Water	Water	Water	Water
300	Water	Water	Water	Water
325	Water	o-xylene	o-xylene	o-xylene
350	Water	Water	Water	Water

References

[1] F. Tchanche B, Pétrissans M, Papadakis G. Heat resources and organic Rankine cycle machines. Renewable and Sustainable Energy Reviews. 2014;39:1185-99.
[2] Kanoglu M. Exergy analysis of a dual-level binary geothermal power plant Geothermics 2002;31:709 - 24.
[3] Stijepovic MZ, Papadopoulos AI, Linke P, Grujic AS, Seferlis P. An exergy composite curves approach for the design of optimum multi-pressure organic Rankine cycle processes. Energy. 2014;69:285-98.
[4] Franco A, Villani M. Optimal design of binary cycle power plants for water-dominated, medium-temperature geothermal fields Geothermics 2009;38:379 - 91.
[5] Schuster A, Karellas S, Aumann R. Efficiency optimization potential in supercritical Organic Rankine Cycles Energy 2010;35:1033 - 9.
[6] Smith IK. Development of the trilateral flash cycle system Part1: fundamental considerations. Proceedings of the Institution of Mechanical Engineers, Part A: Journal of Power and Energy. 1993.
[7] Fischer J. Comparison of trilateral cycles and organic Rankine cycles Energy 2011;36:6208 - 19.
[8] Lai NA, Fischer J. Efficiencies of power flash cycles. Energy. 2012;44:1017-27.
[9] Zamfirescu C, Dincer I. Thermodynamic analysis of a novel ammonia water trilateral Rankine cycle. Thermochimica Acta 2008;477:7 - 15.
[10] Karellas S, Schuster A, Leontaritis A-D. Influence of supercritical ORC parameters on plate heat exchanger design. Applied Thermal Engineering. 2012;33–34:70-6.
[11] Saleh B, Koglbauer G, Wendland M, Fischer J. Working fluids for low-temperature organic Rankine cycles Energy 2007;32:1210 - 21.
[12] Shengjun Z, Huaixin W, Tao G. Performance comparison and parametric optimization of subcritical Organic Rankine Cycle (ORC) and transcritical power cycle system for low-temperature geothermal power generation Applied Energy 2011;88:2740 - 54.
[13] Baik Y-J, Kim M, Chang KC, Kim SJ. Power-based performance comparison between carbon dioxide and R125 transcritical cycles for a low-grade heat source Applied Energy 2011;88:892 - 8.
[14] Lecompte S, van den Broek M, De Paepe M. Thermodynamic analysis of the partially evaporating trilateral cycle. 2nd International Seminar on ORC Power Systems. Rotterdam2013.
[15] Lecompte S, Ameel B, Ziviani D, van den Broek M, De Paepe M. Exergy analysis of zeotropic mixtures as working fluids in Organic Rankine Cycles. Energy Conversion and Management. 2014;85:727-39.
[16] Bell IH, Wronski J, Quoilin S, Lemort V. Pure and Pseudo-pure Fluid Thermophysical Property Evaluation and The Open-Source Thermophysical Property Library Coolprop. Industrial & Engineering Chemistry Research. 2014;53:2498-508.
[17] Lai NA, Wendland M, Fischer J. Working fluids for high-temperature organic Rankine cycles. Energy. 2011;36:199-211.
[18] Maraver D, Royo J, Lemort V, Quoilin S. Systematic optimization of subcritical and transcritical organic Rankine cycles (ORCs) constrained by technical parameters in multiple applications. Applied Energy. 2014;117:11-29.
[19] Ugray Z, Lasdon L, Plummer J, Glover F, Kelly J, Rafael M. Scatter Search and Local NLP Solvers, A multistart Framework for Global Optimization. INFORMS Journal on Computing. 2007;19:238-340.
[20] Byrd RH, Gilbert JC, Nocedal J. A trust region method based on interior point techniques for nonlinear programming. Mathematical Programming. 2000;89:149-85.